PLOS ONE

RESEARCH ARTICLE

Impact of galvanic vestibular stimulation electrode current density on brain current flow patterns: Does electrode size matter?

Dennis Q. Truong[1]*, Alexander Guillen[1], Mujda Nooristani[2,3,4], Maxime Maheu[2,3], Francois Champoux[2,3,4], Abhishek Datta[1,5]

1 Research and Development, Soterix Medical, Woodbridge, NJ, United States of America, **2** Faculty of Medicine, School of Speech-Language and Audiology, University of Montreal, Montreal, QC, Canada, **3** Institut Universitaire sur la Réadaptation en Déficience Physique de Montréal (IURDPM), Pavillon Laurier, CIUSSS du Centre-Sud-de-L'Île-de-Montréal, Montréal, QC, Canada, **4** Centre de Recherche de l'Institut Universitaire de Gériatrie de Montréal, Montréal, Québec, Canada, **5** City College of New York, New York, NY, United States of America

* dtruong@soterixmedical.com

Citation: Truong DQ, Guillen A, Nooristani M, Maheu M, Champoux F, Datta A (2023) Impact of galvanic vestibular stimulation electrode current density on brain current flow patterns: Does electrode size matter? PLoS ONE 18(2): e0273883. https://doi.org/10.1371/journal.pone.0273883

Editor: Mohammad Ali Salehinejad, Leibniz-Institut fur Arbeitsforschung an der TU Dortmund, GERMANY

Received: August 15, 2022

Accepted: January 10, 2023

Published: February 3, 2023

Data Availability Statement: All relevant data are within the paper and its supporting information files.

Funding: 1) Initial who received award: AD 2) Grant number: W912CG21C0014 3) Full name of funder: Department of Defense 4) URL of funder: https://www.darpa.mil/ 5) The funders had no role in the study design,data collection and analysis, decision to publish, or preparation of the manuscript.

Abstract

Background

Galvanic vestibular stimulation (GVS) uses at least one electrode placed on the mastoid process with one or multiple placed over other head areas to stimulate the vestibular system. The exact electrode size used is not given much importance in the literature and has not been reported in several studies. In a previous study, we compared the clinical effects of using different electrode sizes (3 cm^2 and 35 cm^2) with placebo but with the same injected current, on postural control. We observed significant improvement using the smaller size electrode but not with the bigger size electrode. The goal of this study was to simulate the current flow patterns with the intent to shed light and potentially explain the experimental outcome.

Methods

We used an ultra-high-resolution structural dataset and developed a model to simulate the application of different electrode sizes. We considered current flow in the brain and in the vestibular labyrinth.

Results

Our simulation results verified the focality increase using smaller electrodes that we postulated as the main reason for our clinical effect. The use of smaller size electrodes in combination with the montage employed also result in higher induced electric field (E-field) in the brain.

Competing interests: DQT, AG, and AD are employees of Soterix Medical. The remaining authors declare that the research was conducted in the absence of any commercial or financial relationships that could be construed as a potential conflict of interest. This does not alter our adherence to PLOS ONE policies on sharing data and materials.

Conclusions

Electrode size and related current density is a critical parameter to characterize any GVS administration as the choice impacts the induced E-field. It is evident that the higher induced E-field likely contributed to the clinical outcome reported in our prior study.

Introduction

Galvanic Vestibular Stimulation (GVS) is a non-invasive stimulation technique that uses weak electrical current (< 5 mA) to modulate underlying vestibular afferent nerve fibers [1]. This technique has been used in various medical and non-medical applications for more than 100 years [1]. In medical research settings, GVS has shown promising results in diagnosing vestibular disorders as well as treating a wide range of nervous system diseases (e.g.,vestibulopathy, Meniere's disease, gait abnormalities, etc.) [2]. GVS is characterized by different montages and by a constellation of parameters such a waveform type (e.g., DC, sine, sum of sines, noisy GVS), frequency, stimulation duration, etc [3–5]. Classical GVS produces stereotyped automatic perceptual postural and ocular responses by activating both primary otolithic neurons and primary semicircular canal neurons [1,2,6,7].

To characterize the safety and efficacy of any electrical stimulation technique, current density (i.e. current / area) is considered a critical technical parameter. High current densities are often associated with increased sensitivity but when threshold limits are exceeded, it can lead to brain injury [8]. While this is true, our group has also shown that appropriate choice of electrode material and design can be used to deliver high *electrode* current density without pain [9]. Herein, lies an important consideration that often gets overlooked and receives sparse attention in the literature. Electrode current density and the resulting *brain* current density, even though correlated due to the electrode placement, are intrinsically in-dependent stimulation metrics. In the context of a similar non-invasive electrical stimulation technique called transcranial direct current stimulation (tDCS), Nitsche and colleagues demonstrated that a current density value of 1 mA / 35 cm^2 "standardizes" cortical response [10]. This aforementioned value, is however, closely related to the considered electrode montage and does not hold under all conditions. We discuss the potential limitation of this standardized current density value in Datta et al. [11]. Briefly, when two electrodes with the same injected electrode current density are placed immediately adjacent to each other (for instance, 1 cm away), dominant current flow shunts across the scalp leading to no underlying brain flow, thereby leading to no clinical / behavioral response. Another example is current delivery through electrophysiological electrodes (microelectrodes) matched to the standardized current density (0.0001 mA / 0.00035 cm^2 same as 1mA / 35 cm^2) will continue to be ineffective because of the inherently low current intensity value. Therefore, when comparing electrode montages with respect to corresponding effective dose delivery, it is worthwhile to match the brain (and not electrode) electric field (E-field) / current density.

Our group investigated the direct effect of electrode current density in a clinical study to shed more light on this issue [12]. For the first time, we considered two different electrode sizes in a GVS study. Specifically, we tested postural control in a 3 group parallel design (sham, subjects stimulated with a 3 cm^2 electrode area, and subjects stimulated with 35 cm^2 electrode area). A total of 36 patients (age: 20.5–27 years) were recruited with 12 in each group. Each patient received 1 mA and therefore different current density was delivered to the two active groups. The stimulation duration was set to 30 minutes. For the sham group, current was

ramped up to 1 mA for 30 seconds and then gradually decreased to mimic the skin sensation of the active arms. Our results indicated that postural stability can be significantly improved with the 3 cm^2 size electrodes, but not with the 35 cm^2 size electrodes. We postulated that the use of smaller electrodes perhaps resulted in more focal current delivery to the vestibular organs to explain the clinical outcome. Other groups have also demonstrated the utility of GVS as a strategy to enhance postural balance in a range of populations- elderly healthy [13], patients with bilateral vestibular failure [14] to Parkinson's disease [15]. A recent review of the effect of GVS on postural balance (restricted to Parkinson's disease) concluded favorable effect but suggested caution due to limited studies as well as inconsistent methodological details across them [16].

The goal of the current study was to simulate current flow patterns under both of the above active conditions used in our study and to explore whether the use of smaller electrodes did indeed lead to more focal delivery. We consider an ultra-high-resolution model and determine current flow pattern on the cortical surface, and the two implicated structures for GVS mechanism of action (otolith and the semicircular canals).

The importance of electrode size in shaping cortical electric field patterns have been studied previously using computational models in the context of tDCS [17–19] and electroconvulsive therapy (ECT) [20]. With respect to GVS, there are none prior efforts looking specifically at electrode size. However, computational forward modeling has been employed to investigate electrode configurations via a model of the human inner ear [21]. In addition, there exists a whole human head model-based current flow analysis which is a prior effort by our group [22].

Methods

The ultra-high resolution head (MIDA: Multimodal Imaging-Based Detailed Anatomical Model) available through the IT'IS Foundation was used in this study [23]. This dataset was suitable for this study because its resolution (500 μm isotropic) allows visualization and therefore analysis of the small vestibular regions of the head. Further, as noted by the authors in the study, the ear regions were possible to capture due to the incorporation of a heavily T2-weighted MRI slab with high nerve contrast containing these regions. The simulation workflow was largely based on previous work of our group [22,24,25]. These steps were:

1. Image-processing and segmentation of the data. First, the NIFTI (.nii) color masks from the MIDA dataset were processed in MATLAB to generate corresponding tissue masks based on the intensity values. Therefore, all tissue masks including the ones corresponding to the ear regions and cranial nerves reflected the segmentation The resulting masks were imported into Simpleware (Synopsys Ltd., CA, USA) to correct anatomical and continuity errors. Masks containing similar electrical conductivity (e.g. the skull dipole, outer table, and the mandible make up the bone mask) were combined to form a single mask, except for the areas of interest (e.g., vestibular area) through which current flow analysis was to be performed.

2. Replicating electrode geometry and placement. Two different electrode sizes were modeled in Simpleware to mimic the 3.14 cm^2 (1 cm radius) and 35 cm^2 (5 x 7 cm) application used experimentally (Fig 1). The geometry of the electrodes were circular and rectangular, respectively. We refer to the smaller electrode as a 3 cm^2 electrode for simplicity—similar to the clinical study [12]. The shape of the gel remained the same as that of the electrodes. The thickness ratio for both electrode sizes relative to the gel was 0.5:1. The electrodes and gel

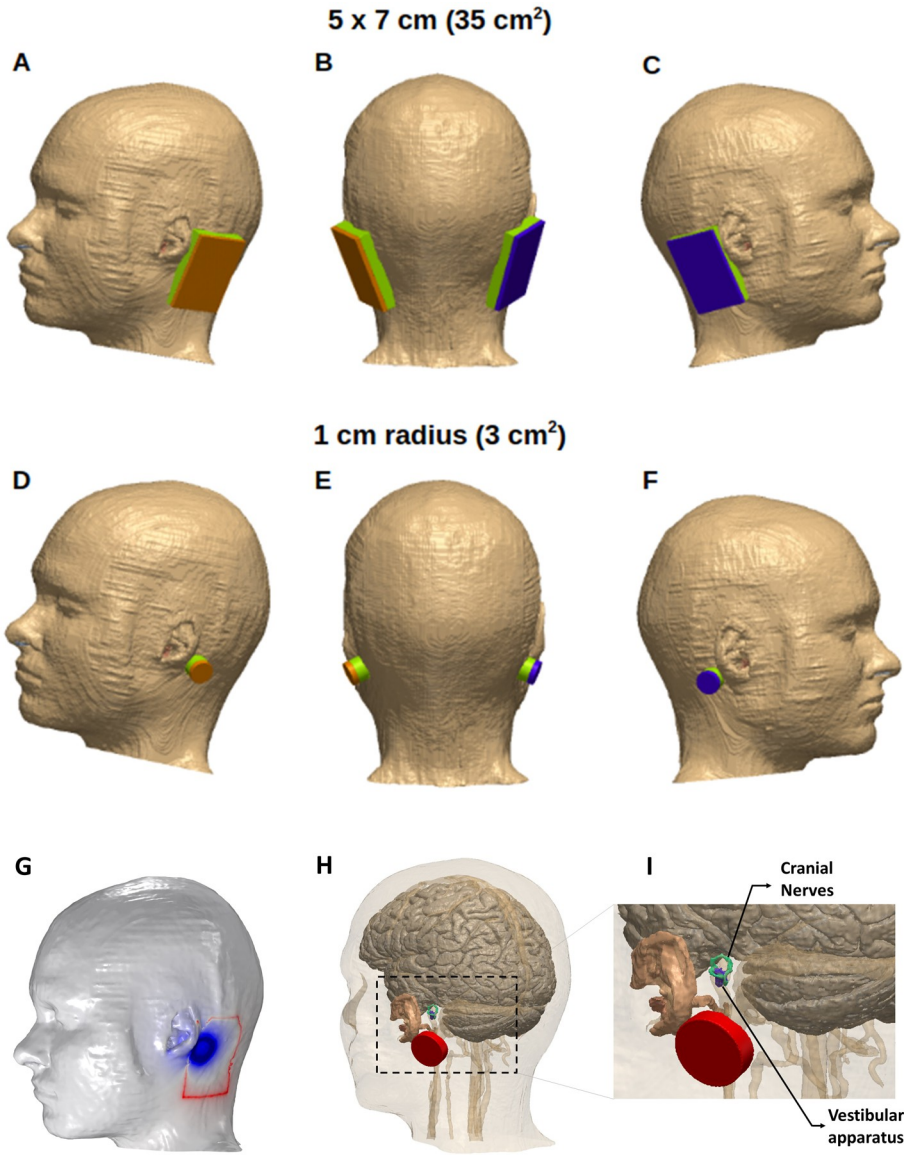

Fig 1. Electrode placements and model detail. Two different electrode sizes were simulated to apply GVS: 35 cm^2 **(A-C)** and ~3 cm^2 **(D-F).** The electrodes were placed on the skin-tissue mask in a Bilateral-Bipolar configuration. **(G):** The two electrode sizes were overlaid on the same head model geometry to highlight final placement with respect to the anatomy. **(H):** To highlight the region of interest in the model geometry with respect to other tissues and the stimulation electrode, certain tissue masks were made semi-transparent. **(I):** The dashed section in (H) is expanded to further highlight model detail.

https://doi.org/10.1371/journal.pone.0273883.g001

were then placed on the mastoid area of the skin tissue mask in a Bilateral-Bipolar configuration as illustrated in Fig 1.

3. Meshing and Finite element method (FEM) model generation. The two different models (corresponding to the two electrode sizes) and each of the segmented tissue compartments/masks were adaptively meshed using Simpleware. The mesh was imported into COMSOL Multiphysics 5.6 (COMSOL Inc., MA, USA) for finite element analysis of current flow. Subsequently induced electrical field (E-field) surface plots of the regions of interest were generated for evaluation.

The isotropic and homogeneous electrical conductivity value in S/m assigned to each mask were: skin (0.465), skull (0.01), cerebrospinal fluid (CSF) (1.65), gray matter (0.276), white matter (0.126), air (1e-7), cranial nerves (0.017126), ear auricular cartilage (0.16113), ear semi-circular canals (2), blood (0.7), gel (1.4), and electrodes (5.8e7) [21,24,26].

The noisy GVS waveform considered in our clinical study involved a spectrum ranging from 0 to 640 Hz [27]. Simulating application of any waveform with frequency content requires consideration of a modified Laplace equation incorporating a reactive component [28]. However, given the real component (i.e. conductivity) dominates at frequencies up to 10 kHz, the standard Laplace equation is used:

$$\nabla \cdot (\sigma \nabla V) = 0$$

where σ: tissue conductivity and V: voltage. The model physics was therefore formulated with the Laplace equation with the following boundary conditions: 1) normal current density condition for the left (anode) electrode corresponding to 1 mA, 2) ground or V = 0 at the right (cathode) electrode, and 3) all external surfaces treated as insulated. The default iterative solver (conjugate gradient) was used to solve for voltage throughout the volume.

Results

For each model considered in this study, the induced E-field / current density plots of the brain and vestibular regions were obtained, as shown in Fig 2. We further overlaid current flow streamlines induced due to both models (Fig 2-C1) and generated a difference plot on the regions of interest (Fig 2-C2 and 2-C3) to analyze potential differences in a systematic fashion. The current flow profile of the Bilateral-Bipolar montage is lateral (left to right) as expected. The simulations confirm that the current entering from one mastoid location at the anode electrode traverses all intermediate tissues until it reaches the brain, and then exits at the second mastoid location at the contralateral cathode electrode side. Fig 2-A2 and 2-B2 indicate that the dominant current flow occurs at the cerebellum and the brain stem region, with some flow in the temporal regions for the model using smaller electrodes. Further, current flow is largely minimal (< 0.1 V/m) in the frontal, parietal and motor cortical regions of the brain.

The predicted maximum E-field (based on the 99th percentile) delivered to the brain using 3 cm^2 electrodes is 0.175 V/m (Fig 2-B2) and the maximum E-field delivered to the brain using 35 cm^2 electrodes is 0.147 V/m (Fig 2-A2). The current streamlines help visualize the entry of current through the mastoid region using both models (Fig 2-A1 and 2-B1). It can be clearly seen that in the case of the 3 cm^2 electrodes, a restricted entry point leads to an increased concentration of the lines of force at the mastoid locations. Additionally, smaller-sized electrodes result in a greater separation between the electrodes (due to greater edge to edge or perimeter to perimeter distance), which results in the current having a lower "motivation" to flow around the back or around the front of the head. Therefore, the net effect of delivering current through smaller-sized electrodes is not only focal delivery, but higher current intensity reaching regions of interest in the brain. In the case of the 35 cm^2 electrodes, the current entry in the mastoids by default is not as concentrated and, due to the smaller effective distance between the electrodes, there is more "current loss" from the back of the head than from the front of the head. This phenomena is clearly highlighted by the higher number of streamlines running from one electrode to the other across the back of the head (Fig 2-A1) and some running around the front of the head. As well, this is further emphasized by the overlay images of the two simulations (Fig 2-C1) that illustrates the focal entry and dominant lateral flow of the blue (3 cm^2) as opposed to the red streamlines (35 cm^2).

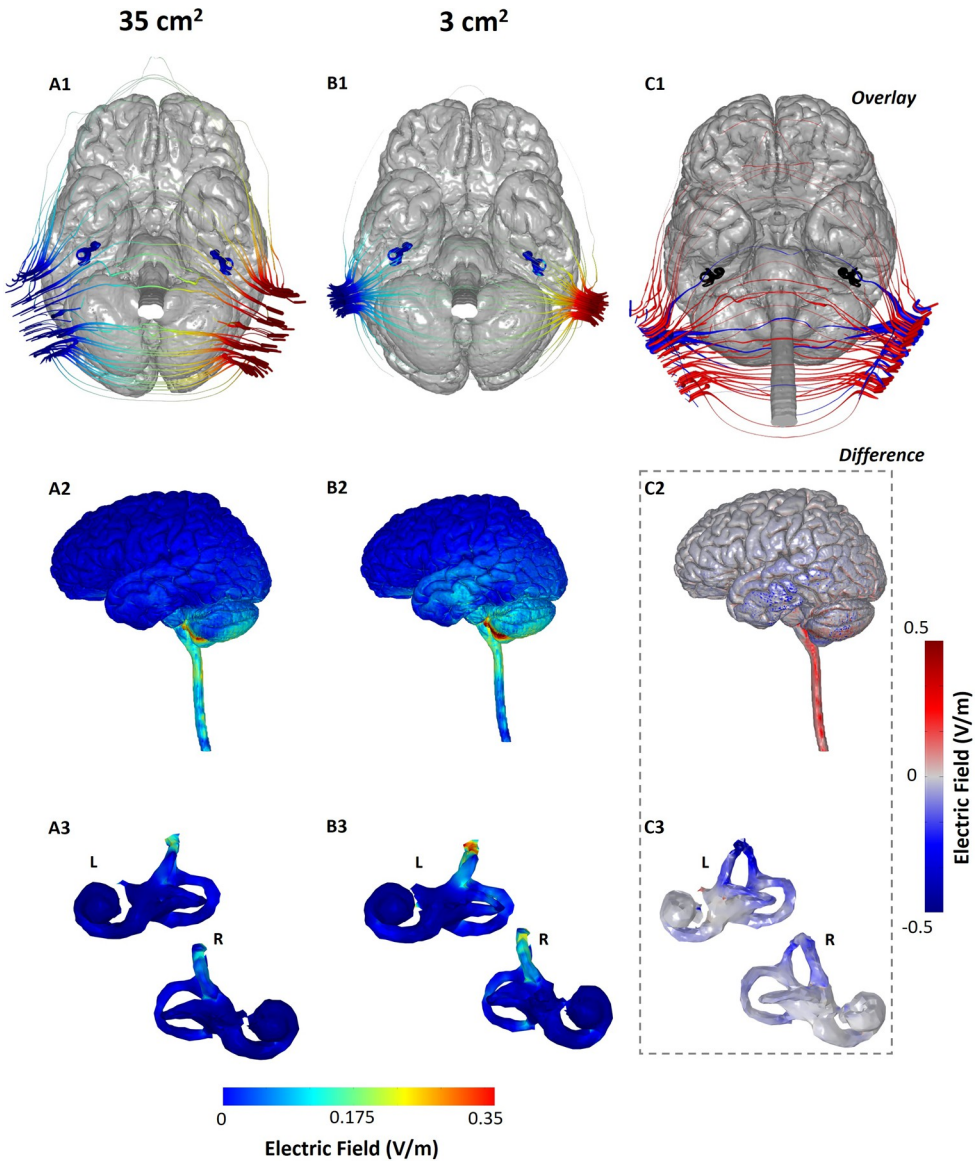

Fig 2. Comparison of GVS induced current flow using small- and large-size electrodes. Columns A (A1, A2, A3) and B (B1, B2, B3) correspond to the 35 cm^2 and 3 cm^2 electrodes, respectively. The current streamlines from both models are overlaid in C1. C2 and C3 indicate the difference in induced E-field due to the two electrode sizes. The first row (A1, B1 and C1) shows the current streamline plots with the brain, SCC and otolith organs masks visible to provide enhanced visualization of current flow with respect to their anatomy. The second row (A2, B2, and C2) shows the induced brain surface E-field plots. Similarly, the third row (A3, B3, and C3) shows the induced E-field plots on the vestibular labyrinth.

https://doi.org/10.1371/journal.pone.0273883.g002

While current input is restricted at the level of the skin and the skull, we actually observe higher current flow in the temporal cortex using the 3 cm^2 electrodes. This is counter-intuitive but supported by the overall current flow pattern due to any transcranial electrical stimulation modality. The scalp and the CSF are the most conductive tissues in the head. When current is first injected at the level of the scalp, there is some shunting (i.e. flow *across* the skin rather than *into* the tissue) due to its higher conductivity with respect to the underlying skull [9]. The extent of this shunting is determined by the electrode montage. The remaining current entering the skull largely flows into the next tissue (CSF), as there is less incentive for current to

flow across the low conductive skull. Since less current shunt (loss) occurs at the scalp level in the 3 cm^2 electrode, the magnitude of the current entering the CSF is higher compared to the current entering the CSF with the 35 cm^2 electrodes. In summary, a combination of the aforementioned factors explains why higher current flow is observed at the temporal cortex due to the smaller sized electrodes. For the larger electrodes, as there is more current loss across the scalp, there is more inferior current flow. This is evident in the observed E-field magnitude (~0.3 V/m) in regions extending along the spinal cord. This is further emphasized via the difference image (Fig 2-C2) that indicates that the 3 cm^2 electrode model results in more flow in the cerebellum and the temporal regions (blue hue), whereas, the 35 cm^2 electrode model results in more flow in the brain stem regions (red hue).

When evaluating flow at the level of the vestibular end organs, similar flow (spatial distribution) but higher induced E-field (Fig 2-B3) was observed for the model simulating smaller electrodes. For both models, we observe increased current flow in the anterior canals with respect to the lateral and posterior canals. The maximum E-field delivered to the left vestibular network with the 35 cm^2 and 3 cm^2 electrodes was 0.126 V/m and 0.201 V/m respectively. Similarly, when considering the right network, the induced E-field is 0.108 V/m when using 35 cm^2 electrodes and 0.165 V/m when using the 3 cm^2 electrodes. The relative E-field percentage increase (Table 1) indicates a slightly higher value for the left network. This can be expected as the head anatomy is not perfectly symmetric (with respect to the sagittal plane) and therefore, variations in current flow will manifest in different percentage increases.

Discussion

The predictions in this study verify the focality increase that we previously proposed as the primary reason for the postural control improvement using smaller size electrodes [12]. The concentrated current entry into the head in combination with the montage employed, in fact, results in more current entering the brain—resulting in higher induced E-field in the brain and the vestibular labyrinth. While induced E-field magnitude in the target of interest is one of the main drivers of neuromodulation, a one-to-one linear translation of clinical / behavioral effects is not expected due to several factors. It is for this reason that clinical effects with 2 mA current injection for instance, are not expected to simply double from the effects observed at 1 mA—as observed from tDCS studies [29]. Nonetheless, it is well accepted that neuronal modulation is directly related to the induced E-field. This has been extensively demonstrated by a multitude of experimental and theoretical studies indicating that polarization of short or bent cortical axons [30,31] and synaptic efficacy vary linearly with E-field magnitude [32] and neuronal excitability metrics vary with E-field magnitude [32,33]. We are therefore able to conclude that the higher induced E-field contributed in some fashion to the improvement in postural stability. We also note that the increases in induced E-field in cortical (19%) and vestibular regions (52–59%) with the smaller electrodes are in the same order of percentage improvement of the clinical effects. Taken together, our results offer a plausible explanation of the experimental findings in Nooristani et al. [12]. In summary, we demonstrate the importance of electrode size and encourage the community to accurately document dimensions in

Table 1. Maximum induced E-field (based on 99th percentile) in the brain and vestibular regions across the two models. The percentage increase of E-field with respect to the larger electrode model is noted in the final column.

Electric field (V/m)	35 cm^2	3 cm^2	$(E_3 - E_{35}) / E_{35}$
Brain (White and gray matter)	0.147	0.175	19.05%
Left vestibular region	0.126	0.201	59.52%
Right vestibular region	0.108	0.165	52.78%

https://doi.org/10.1371/journal.pone.0273883.t001

their publications. While not the focus here, one can foresee that electrodes with different shapes but same size in terms of area (e.g. 2 cm x 17.5 cm strip versus 5 x 7 cm rectangle) may also lead to different induced E-field patterns. Therefore, all electrode details (size, shape, conductive medium and related contact area, etc.) for a given electrode montage must be documented. Moreover, this information is central to ensure replicability of studies thereby helping drive true determination of clinical utility.

Our finding that the anterior canals receive greater current flow with the Bilateral-Bipolar montage (irrespective of the electrode size used) would imply greater sensitivity of the canal with respect to the lateral and the posterior canal. This finding could potentially be used to further adjust weights of the vector summation model proposed by Day et al. [34]. In general, a future research topic could be to use current flow model predictions as used here across different GVS electrode montages to test resultant impact on the vector summation model's accuracy. We also note that calibration of current intensity is frequently used in GVS administration where individualized intensity is delivered based on the subjects' perceptual threshold. The static field approximation in our model implies linearity of the solution and therefore induced E-field will scale linearly with the stimulation magnitude. So the induced cortical E-field for 0.7 mA scalp current will be simply 0.7 times the cortical E-field induced for 1 mA. Further, it is important to keep in mind that precise E-field values for a particular subject can only be determined when considering individual MRI and repeating the computation as presented here. The MIDA dataset is a specific template developed using specialized sequences, and as mentioned previously, specifically optimized to enhance the ear structures. The availability of these structures were critical in performing the necessary analysis and evaluation. While, naturally it cannot capture inter-individual variation in induced current flow [24], it allows for isolating the effects of electrode size- the central goal of this study.

In summary, computational modeling can be used to support GVS administration in several ways similar to efforts transforming other modalities (DBS, TMS, etc) [35,36]. As research using GVS increases and evolves, there is potential to leverage modeling to help with determining optimal parameters (electrode location, electrode shape, etc.), relate current flow to stimulation outcome, perform safety analysis, etc. We expect this study to help demonstrate this utility and encourage additional efforts.

Supporting information

S1 Data.
(ZIP)

Author Contributions

Conceptualization: Dennis Q. Truong, Abhishek Datta.

Data curation: Dennis Q. Truong, Alexander Guillen.

Formal analysis: Dennis Q. Truong, Alexander Guillen, Abhishek Datta.

Funding acquisition: Abhishek Datta.

Investigation: Dennis Q. Truong.

Methodology: Dennis Q. Truong, Mujda Nooristani, Maxime Maheu, Francois Champoux, Abhishek Datta.

Project administration: Abhishek Datta.

Resources: Abhishek Datta.

Visualization: Dennis Q. Truong.

Writing – original draft: Alexander Guillen, Abhishek Datta.

Writing – review & editing: Dennis Q. Truong, Alexander Guillen, Mujda Nooristani, Maxime Maheu, Francois Champoux, Abhishek Datta.

References

1. Wardman DL and Fitzpatrick RC. What does Galvanic Vestibular Stimulation stimulate? Adv Exp Med Biol 2002; 508:119–28. https://doi.org/10.1007/978-1-4615-0713-0_15 PMID: 12171101
2. Dlugaiczyk J, Gensberger KD, Straka H. Galvanic vestibular stimulation: from basic concepts to clinical applications. J Neurophysiol 2019; 121 (6):2237–2255. https://doi.org/10.1152/jn.00035.2019 PMID: 30995162
3. Aoyama K, Iizuka H, Ando H, Maeda T. Four-pole galvanic vestibular stimulation causes body sway about three axes. Sci Rep. 2015 May 11; 5:10168. https://doi.org/10.1038/srep10168 PMID: 25959790
4. Cevette MJ, Stepanek J, Cocco D, Galea AM, Pradhan GN, Wagner LS, et al. Oculo-vestibular recoupling using galvanic vestibular stimulation to mitigate simulator sickness. Aviat Space Environ Med. 2012 Jun; 83(6):549–55. https://doi.org/10.3357/asem.3239.2012 PMID: 22764608
5. Mulavara AP, Fiedler MJ, Kofman IS, Wood SJ, Serrador JM, Peters B, et al. Improving balance function using vestibular stochastic resonance: optimizing stimulus characteristics. Exp Brain Res. 2011 Apr; 210(2):303–12. https://doi.org/10.1007/s00221-011-2633-z PMID: 21442221
6. Kim J. (2013). Head movements suggest canal and otolith projections are activated during galvanic vestibular stimulation. Neuroscience, 253, 416–425. https://doi.org/10.1016/j.neuroscience.2013.08.058 PMID: 24021920
7. Curthoys I. S., & Macdougall H. G. (2012). What galvanic vestibular stimulation actually activates. Frontiers in neurology, 3, 117. https://doi.org/10.3389/fneur.2012.00117 PMID: 22833733
8. Nitsche MA, Liebetanz D, Lang N, Antal A, Tergau F, Paulus W. Safety criteria for transcranial direct current stimulation (tDCS) in humans. Clin Neurophysiol. 2003 Nov; 114(11):2220–2; author reply 2222–3. https://doi.org/10.1016/s1388-2457(03)00235-9 PMID: 14580622
9. Datta A, Bansal V, Diaz J, Patel J, Reato D, Bikson M. Gyri-precise head model of transcranial direct current stimulation: improved spatial focality using a ring electrode versus conventional rectangular pad. Brain Stimul. 2009 Oct; 2(4):201–7, 207.e1. https://doi.org/10.1016/j.brs.2009.03.005 PMID: 20648973
10. Nitsche MA, Doemkes S, Karaköse T, Antal A, Liebetanz D, Lang N, et al. Shaping the effects of transcranial direct current stimulation of the human motor cortex. J Neurophysiol. 2007 Apr; 97(4):3109–17. https://doi.org/10.1152/jn.01312.2006 PMID: 17251360
11. Datta A, Elwassif M, Battaglia F, Bikson M. Transcranial current stimulation focality using disc and ring electrode configurations: FEM analysis. J Neural Eng. 2008 Jun; 5(2):163–74. https://doi.org/10.1088/1741-2560/5/2/007 PMID: 18441418
12. Nooristani M et al., The importance of nGVS current density for postural control enhancement, Brain Stimulation, https://doi.org/10.1016/j.brs.2019.07.022 PMID: 31395519
13. Fujimoto Y. Yamamoto T. Kamogashira M. Kinoshita N. Egami Y. Uemura F. et al. Iwasaki, Noisy galvanic vestibular stimulation induces a sustained improvement in body balance in elderly adults, Sci. Rep. 6 (1) (2016) 1–8 https://doi.org/10.1038/srep37575.
14. Max Wuehr J. Decker R. Schniepp, Noisy galvanic vestibular stimulation: an emerging treatment option for bilateral vestibulopathy, J. Neurol. 264 (Suppl. 1) (2017) 81–86, https://doi.org/10.1007/S00415-017-8481-4.
15. Kataoka H, Okada Y, Kiriyama T, Kita Y, Nakamura J, Morioka S, et al. Can Postural Instability Respond to Galvanic Vestibular Stimulation in Patients with Parkinson's Disease? J Mov Disord. 2016 Jan; 9(1):40–3. https://doi.org/10.14802/jmd.15030 PMID: 26648182
16. Mahmud M, Hadi Z, Prendergast M, Ciocca M, Saad AR, Pondeca Y, Tai Y, Scott G, Seemungal BM. The effect of galvanic vestibular stimulation on postural balance in Parkinson's disease: A systematic review and meta-analysis. J Neurol Sci. 2022 Nov 15; 442:120414. https://doi.org/10.1016/j.jns.2022.120414 Epub 2022 Sep 9. PMID: 36116217.
17. Bikson M, Datta A, Rahman A, Scaturro J. Electrode montages for tDCS and weak transcranial electrical stimulation: role of "return" electrode's position and size. Clin Neurophysiol. 2010 Dec; 121 (12):1976–8. https://doi.org/10.1016/j.clinph.2010.05.020 PMID: 21035740

18. Faria P, Hallett M, Miranda PC. A finite element analysis of the effect of electrode area and inter-electrode distance on the spatial distribution of the current density in tDCS. J Neural Eng. 2011 Dec; 8 (6):066017. https://doi.org/10.1088/1741-2560/8/6/066017 PMID: 22086257

19. Saturnino GB, Antunes A, Thielscher A. On the importance of electrode parameters for shaping electric field patterns generated by tDCS. Neuroimage. 2015 Oct 15; 120:25–35. https://doi.org/10.1016/j.neuroimage.2015.06.067 PMID: 26142274

20. Deng ZD, Lisanby SH, Peterchev AV. Controlling stimulation strength and focality in electroconvulsive therapy via current amplitude and electrode size and spacing: comparison with magnetic seizure therapy. J ECT. 2013 Dec; 29(4):325–35. https://doi.org/10.1097/YCT.10.1097/YCT.0b013e3182a4b4a7 PMID: 24263276

21. Schier P, Handler M, Johnson Chacko L, Schrott-Fischer A, Fritscher K, Saba R, et al. Model-Based Vestibular Afferent Stimulation: Evaluating Selective Electrode Locations and Stimulation Waveform Shapes. Front Neurosci. 2018 Aug 30; 12:588. https://doi.org/10.3389/fnins.2018.00588 PMID: 30214391

22. C. Thomas, D. Truong, T. K. Clark and A. Datta, "Understanding current flow in Galvanic Vestibular stimulation: A Computational Study," 2020 42nd Annual International Conference of the IEEE Engineering in Medicine & Biology Society (EMBC), 2020, pp. 2442–2446.

23. Iacono MI, Neufeld E, Akinnagbe E, et al. MIDA: A multimodal imaging-based detailed anatomical model of the human head and neck. PLoS One. 2015; 10:e0124126. https://doi.org/10.1371/journal.pone.0124126 PMID: 25901747

24. Datta A, Truong D, Minhas P, Parra LC, Bikson M. Inter-Individual Variation during Transcranial Direct Current Stimulation and Normalization of Dose Using MRI-Derived Computational Models. Front Psychiatry. 2012; 3:9.

25. Bikson M and Datta A. Guidelines for precise and accurate computational Brain Stimul. 2012 Jul; 5 (3):430–1.

26. Parazzini M, Rossi E, Ferrucci R, Liorni I, Priori A, Ravazzani P. Modelling the electric field and the current density generated by cerebellar transcranial DC stimulation in humans. Clin Neurophysiol. 2014 Mar; 125(3):577–84. https://doi.org/10.1016/j.clinph.2013.09.039 PMID: 24176297

27. Inukai Y, Masaki M, Otsuru N, Saito K, Miyaguchi S, Kojima S, et al. Effect of noisy galvanic vestibular stimulation in community-dwelling elderly people: a randomized controlled trial. J Neuroeng Rehabil. 2018 Jul 3; 15(1):63. https://doi.org/10.1186/s12984-018-0407-6 PMID: 29970144

28. Thomas C, Truong DQ, Lee K, Deblieck C, Androulakis XM, Datta A. Determination of Current Flow Induced by Transcutaneous Electrical Nerve Stimulation for the Treatment of Migraine: Potential for Optimization. Front Pain Res (Lausanne). 2021 Dec 6; 2:753454. https://doi.org/10.3389/fpain.2021.753454 PMID: 35295421

29. Batsikadze G, Moliadze V, Paulus W, Kuo MF, Nitsche MA. Partially non-linear stimulation intensity-dependent effects of direct current stimulation on motor cortex excitability in humans. J Physiol. 2013 Apr 1; 591(7):1987–2000. https://doi.org/10.1113/jphysiol.2012.249730 PMID: 23339180

30. Tranchina D, Nicholson C. A model for the polarization of neurons by extrinsically applied electric fields. Biophys J. 1986 Dec; 50(6):1139–56. https://doi.org/10.1016/S0006-3495(86)83558-5 PMID: 3801574

31. Maccabee PJ, Amassian VE, Eberle LP, Cracco RQ. Magnetic coil stimulation of straight and bent amphibian and mammalian peripheral nerve in vitro: locus of excitation. J Physiol. 1993 Jan; 460:201–19. https://doi.org/10.1113/jphysiol.1993.sp019467 PMID: 8487192

32. Jefferys JG. Influence of electric fields on the excitability of granule cells in guinea-pig hippocampal slices. J Physiol. 1981; 319:143–52. https://doi.org/10.1113/jphysiol.1981.sp013897 PMID: 7320909

33. Roth BJ. Mechanisms for electrical stimulation of excitable tissue. Crit Rev Biomed Eng. 1994; 22(3–4):253–305. PMID: 8598130

34. Day B.L., Ramsay E., Welgampola M.S. et al. The human semicircular canal model of galvanic vestibular stimulation. Exp Brain Res 210, 561–568 (2011). https://doi.org/10.1007/s00221-011-2565-7 PMID: 21287152

35. Butson CR, McIntyre CC. Role of electrode design on the volume of tissue activated during deep brain stimulation. J Neural Eng. 2006 Mar; 3(1):1–8. https://doi.org/10.1088/1741-2560/3/1/001 PMID: 16510937

36. Deng ZD, Lisanby SH, Peterchev AV. Electric field depth-focality tradeoff in transcranial magnetic stimulation: simulation comparison of 50 coil designs. Brain Stimul. 2013 Jan; 6(1):1–13. https://doi.org/10.1016/j.brs.2012.02.005 PMID: 22483681